

用√符号选择一类	
教 学	
科 研	√
编号（由专家组 填写）	

## 第十一届全国高校物理实验教学研讨会 本科学生物理实验论文评比表

学生姓名： 姚慧明

申报学校： 北京邮电大学

联系方式： 电话： 18810107329

QQ： 3105277239

E-mail： 3105277239@qq.com

填表日期： 2021 年 5 月 22 日

全国高校物理实验教学研讨会组委会制

二〇二〇年一月

学 生 作 者 及 发 表 有 关 物 理 实 验 论 文 情 况	姓名	姚慧明	性别	女	出生年月	2000.07
	学校名称	北京邮电大学				
	入学时间	2017.09	毕业时间	2021.07		
	学号	2017212504				
	参评论文:	(题目. 杂志名称, 卷/期、页、年)				
		Dual-band microstrip antenna based on polarization conversion metasurface structure. Frontiers in Physics, 8、279、2020				
		(注: 论文的第一作者必须为大学本科生, 且其论文研究工作是在本科生阶段完成的, 到现场答辩的为该论文的学生作者之一。)				
		<b>论文作者情况 (按发表论文作者顺序列出):</b>				
		<b>姓名</b>	<b>身份</b>	<b>单位</b>	<b>作用/贡献</b>	
		姚慧明	学生	北京邮电大学	设计天线及撰写论文	
		刘馨艺	学生	北京邮电大学	天线测试	
		朱洪波	副教授	北京邮电大学	提出论文修改意见	
	李海红	教授	北京邮电大学	提出论文修改意见		
	董国艳	副教授	中国科学院大学	提出论文修改意见		
	毕科	教授	北京邮电大学	整体指导		
	<b>简要介绍 (研究背景、问题、方法、创新点、学术及应用价值和引用情况等):</b>					
	<b>研究背景:</b>					
	近年来, 无线通信技术飞速发展, 通信设备在便携式的需求下不断向小型化发展, 而内部的功能却趋向多样化, 这就要求其内置天线有很强的集成能					

力。微带贴片天线具备体积小、结构简单、成本低、易集成等优点，已被广泛应用于各类无线通信设备。

在实际应用中，由于无线频谱资源有限，而且用于无线通信系统的频段各不相同，因而对天线提出了多频化要求。多频段天线不仅可以减少天线个数，缩小设备体积；还可以避免不同频段间的串扰，提高天线工作效率。因此，如何在保证天线整体性能优良的情况下，实现天线的多波段工作，是一个具有重大科学意义的研究课题。

目前实现天线多频化设计的思路主要有两种：一种是通过增加天线的谐振模式来增加新的谐振频点；另外一种是通过增加天线表面电流的流动路径来实现天线的多频段工作。据此来实现多频化天线设计的方法主要包括三种：多枝节技术、开槽技术和可重构技术。其中，多枝节技术和开槽技术的发展更为成熟。

#### **问题：**

传统的实现多频段天线设计的方法主要通过微带天线设计理论来计算各辐射枝节的有效长度，不仅导致天线设计过程较为复杂；而且天线的多频段工作需要通过添加寄生枝节或开槽来实现，使得加工制备较为困难并且难以在系统中集成，从而限制了其实际应用。

#### **方法：**

超表面是一类人工设计的具有奇异电磁特性的二维层状材料，具有天然材料所不具备的超常物理性质，这使其在提高天线性能上有着广阔的发展空间。互补开口谐振环(Complementary Split Ring Resonator, CSRR)是一种常见的超表面结构单元，具有实现小型化的功能而且能够产生较强谐振，将其引入天线设计可有效实现天线的小型化和多频段。在已有的研究中，很多学者将超表面结构加载在天线辐射贴片上或直接将其作为寄生辐射单元，这种方式容易对原有谐振频率产生影响；因此有部分学者尝试在天线地板刻蚀超表面结构，发现由于中间介质基板的阻隔使得对天线原谐振频率的影响有所降低。

鉴于 C 波段应用的广泛性，本文首先设计了一款工作于 C 波段的矩形微带天线。接着通过在天线地板刻蚀互补开口谐振环在 S 波段产生新的谐振频点，从而完成双频超表面微带天线的设计。最后探究互补开口谐振环结构参数和位置参数对天线的回波损耗的影响，以此来完成天线的优化。

#### **实验仪器与装置：**

论文主要进行了数值仿真模拟、样品制备和样品测试三项工作。

首先利用电磁仿真软件 CST 完成天线的设计，其次使用电路板雕刻机刻制天线样品，最后使用矢量网络分析仪来对天线样品进行测试。天线制备和测试仪器如图 1 和 2 所示。

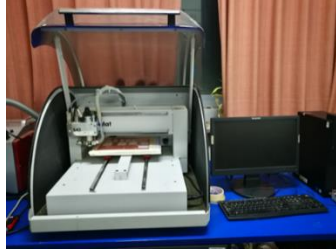


图 1 电路板雕刻机



图 2 矢量网络分析仪

### 数据测量与分析:

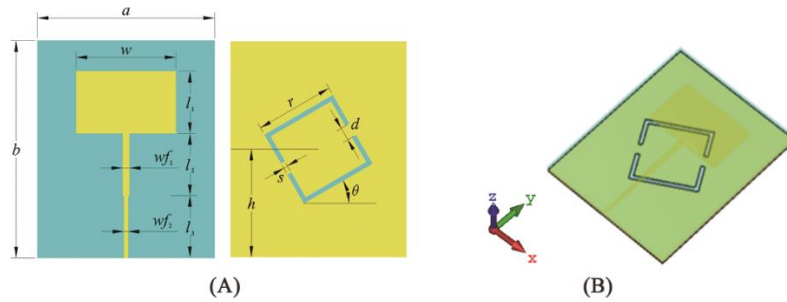


图 3 基于 CSRR 设计的双频微带天线的 (A) 正视图和俯视图 (B) 三维方向图

基于互补开口谐振环设计的双频微带天线结构如图 3 所示。为验证所设计天线在实际中的应用效果，利用电路板雕刻机加工制备优化后的天线样品如图 4 所示。利用矢量网络分析仪测试实物天线电磁性能，其实测与仿真的回波损耗曲线对比如图 5 所示。

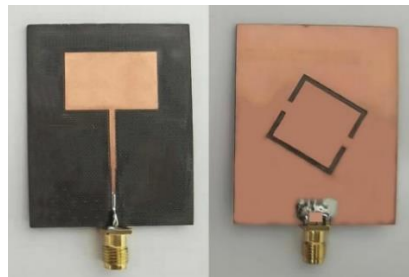


图 4 优化后天线实物

由图 5 可知，测试结果中两个谐振峰的中心频率都产生偏移，谐振频率处的回波损耗值都增加了 3 - 4 dB，而且实测的天线带宽要比仿真宽许多。这是由于在实际加工时精度和测量存在误差所造成的。虽然测试结果与仿真结果相比存在一些误差，但是相较于没有刻蚀 CSRR 结构的微带天线，仍然实现

了双波段工作。说明在天线地板刻蚀 CSRR 结构，可有效实现天线的多频化，证明了天线设计方法的有效性。

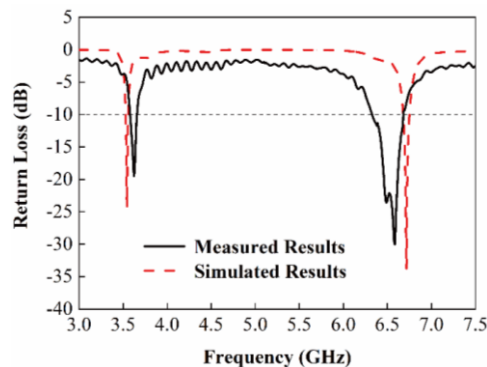


图 5 回波损耗实测与仿真对比曲线

此外，我们还研究了天线在谐振频率处的表面电流分布和辐射方向。分析表明地板上刻蚀的 CSRR 结构与辐射贴片之间具有一定的耦合作用，因此对原来的谐振峰具有一定的影响。但是由于中间隔着一个 1.5 mm 厚的介质基板，具有相应的隔离作用，使得这种影响较小。并且通过一系列结构参数的优化，能够使得谐振频率处的回波损耗得到改善。

#### 创新点：

- (1) 从研究内容上看：本文将超表面结构应用于微带天线设计，在实现天线高性能、小型化的同时，研究天线的多频段实现机制，突破了微带天线贴片长度必须为谐振波长一半的限制，为多频天线的设计提供了新的思路。
- (2) 从研究方法上看：本文采用“数值仿真与实验验证相结合”的方法，首先通过仿真模拟和参数扫描完成天线的设计及优化，然后再进行加工和测试，简化了工艺流程。
- (3) 从研究成果上看：优化后的天线工作频段由 C 波段拓展到 S、C 双波段，满足了天线的多频化需求。同时，优化后的天线在原 C 波段的回波损耗下降了约 40%，改善了天线的阻抗匹配。此外，设计的天线具有超表面的亚波长尺寸优势，简单轻巧，便于制备。

#### 学术及应用价值和引用情况：

本文在深刻理解超表面电磁特性的基础上，将超表面技术与传统天线设计相结合，进而完成多频段天线的设计及优化。基于超表面结构的微带天线设计研究具有较好的理论价值与现实意义，有利于缓解无线电波资源紧缺问题，为多频段天线设计提供了新的思路。





# Dual-Band Microstrip Antenna Based on Polarization Conversion Metasurface Structure

Huiming Yao<sup>1†</sup>, Xinyi Liu<sup>1†</sup>, Hongbo Zhu<sup>1</sup>, Haihong Li<sup>1</sup>, Guoyan Dong<sup>2\*</sup> and Ke Bi<sup>1,3\*</sup>

<sup>1</sup> School of Science, Beijing University of Posts and Telecommunications, Beijing, China, <sup>2</sup> College of Opto-Electronic Technology, University of Chinese Academy of Sciences, Beijing, China, <sup>3</sup> Beijing University of Posts and Telecommunications Research Institute, Shenzhen, China

## OPEN ACCESS

### Edited by:

Xufeng Jing,  
China Jiliang University, China

### Reviewed by:

Xiaojuan Fu,  
Southeast University, China  
Shobhit K. Patel,  
Marwadi University, India  
Fenglong Wang,  
Shandong University, China

### \*Correspondence:

Guoyan Dong  
gydong@ucas.ac.cn  
Ke Bi  
bike@bupt.edu.cn

<sup>†</sup>These authors have contributed  
equally to this work

### Specialty section:

This article was submitted to  
Optics and Photonics,  
a section of the journal  
Frontiers in Physics

Received: 14 May 2020

Accepted: 22 June 2020

Published: 04 September 2020

### Citation:

Yao H, Liu X, Zhu H, Li H, Dong G and  
Bi K (2020) Dual-Band Microstrip  
Antenna Based on Polarization  
Conversion Metasurface Structure.  
Front. Phys. 8:279.  
doi: 10.3389/fphy.2020.00279

A dual-band microstrip patch antenna (MPA) based on a polarization conversion metasurface structure was designed. By etching the complementary split ring resonator (CSRR) on the ground plane, a new resonance frequency is generated. The proposed antenna is obtained through optimizing the structural parameters of CSRR. Compared with the antenna without CSRR, the return loss of the proposed antenna increases by ~40% at the original resonance frequency. The measured results are similar to the simulated results, verifying the reliability of the antenna. This work introduces a new way of designing multi-band antenna.

**Keywords:** microstrip antenna, dual-band, polarization conversion, metasurface structure, complementary split ring resonator

## INTRODUCTION

An antenna plays an important role in modern wireless communication systems. In recent years, the miniaturization and multi-functionalization of communication devices require that the internal antenna has strong integration capabilities [1, 2]. Meanwhile, owing to the lack of wireless spectrum resources, the demand for multi-band antenna has increased [3–5]. Microstrip patch antenna (MPA) are extensively used due to their advantages of small size, simple structure, low cost, and ease of integration [6, 7]. Many methods have been studied to obtain multi-band antenna, such as coupling feed technologies [8], slot-loaded technologies [9], and reconfigurable technologies [10, 11]. Unfortunately, these methods require complex calculation, and the antenna structures are difficult to manufacture. Thus, new designs should be explored to simplify the structure and theoretical analysis.

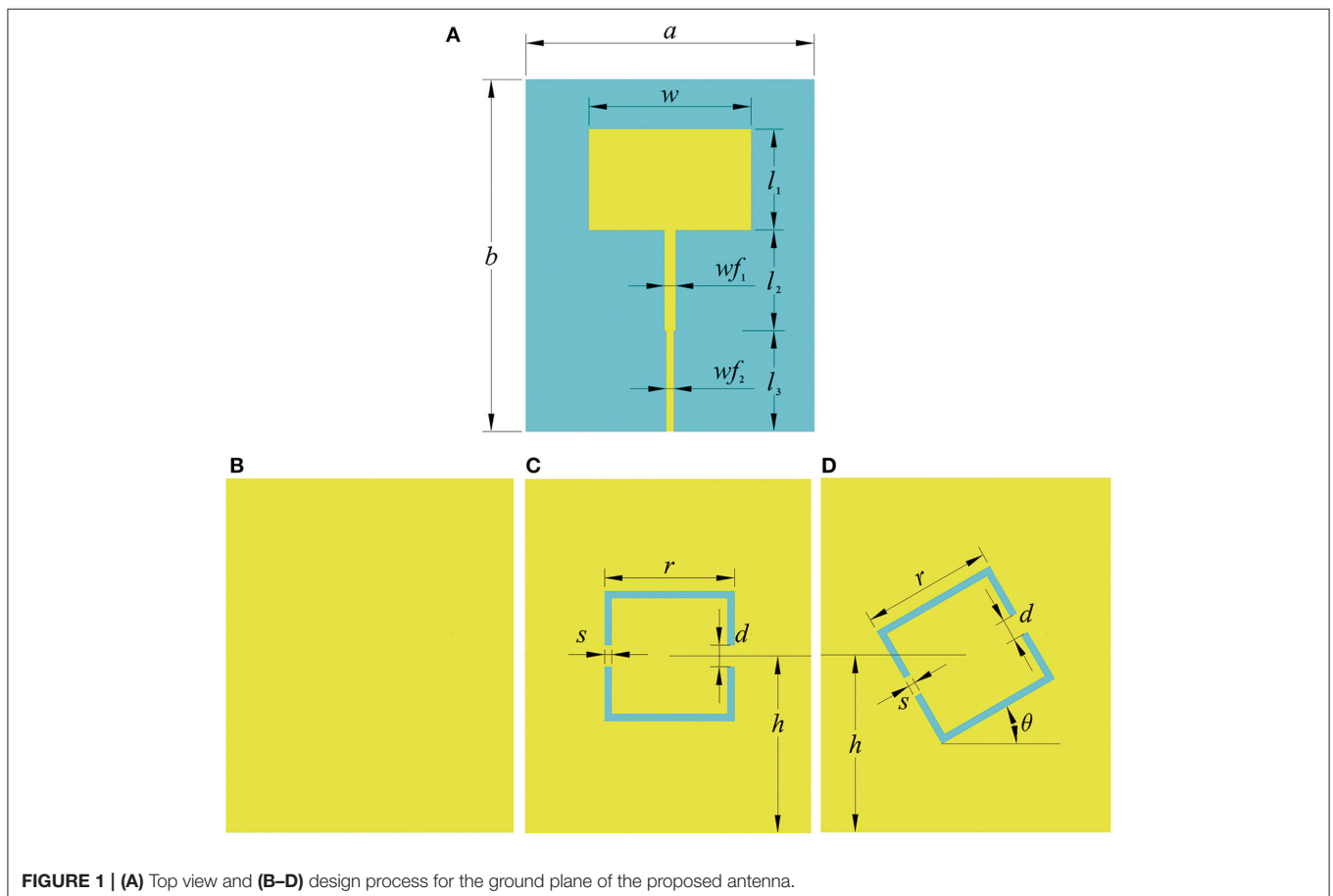
Metasurface, due to its extraordinary electromagnetic properties, is widely used in antenna design [12–14], namely in the realization of multi-band [15, 16], ultra-wide-band [17–19], and high-gain antenna [20, 21]. In most cases, the metasurface structure is loaded on the antenna as a radiating element. The capability of a multi-band operation is not currently apparent. Many efforts have been made to solve this problem, such as etching a complementary split ring resonator (CSRR) on the ground plane. The CSRR unit cell can resonate with an electromagnetic wave, resulting in new resonance peaks. Ali et al. [22] created a triple-band antenna by etching rectangular and circular CSRRs. Zhou et al. [23] fabricated a composite right/left-handed structure as the radiating element and employed a square CSRR to get a dual-band antenna. Xu et al. [24] used a simple square split ring resonator to design an ultra-broad-band linear polarization converter, which provided a way to change the antenna polarization mode. We have recently obtained a broadband microstrip patch antenna by using a complementary rhombus resonator [25].

In this work, we designed a dual-band MPA loaded with a CSRR structure. The CSRR serves as a resonator. From the simulated results, it is found that the MPA exhibits excellent performance within the dual-band resonance in the range of 3.0–7.5 GHz. The measured results are similar to the simulated ones, which proves that the proposed antenna can be well-applied to physical devices.

## ANTENNA DESIGN

C-band antenna have been widely used in satellite communication and navigation [26]. Therefore, we designed an antenna operating at 6.9 GHz. The top and back view of the antenna are, respectively, shown in **Figures 1A,B**. The upper layer of the antenna consists of a rectangular patch, and two different-width feedlines. The middle layer is an FR4 substrate with a relative dielectric constant of 2.65 and the lower layer is a metal ground plane. In order to realize the design of the dual-band antenna, the ground plane is modified. As shown in **Figure 1C**, CSRR was etched on the ground plane which is used to generating new resonance frequency. To further improve the electromagnetic performance of the antenna, a series of parameter optimization was carried out, and the ground plane of the proposed antenna is shown in **Figure 1D**.

The simulated results of the proposed antenna are shown in **Figure 2**, with a series of side length  $r$ , split width  $d$ , rotation angle  $\theta$ , and distance  $h$ . It can be seen that the original resonance frequency is affected by length  $r$ , split width  $d$ , and rotation angle  $\theta$ , while the new resonance frequency is mainly tuned by distance  $h$ . According to **Figure 2A**, as  $r$  increases from 15.0 to 16.5 mm, the original resonance frequency moves to the lower frequency. When  $r = 16.0$  mm, the return loss at the original resonance frequency is maximum. **Figure 2B** demonstrates that, as  $d$  increases from 0 to 4.5 mm, the original resonance frequency moves to the higher frequency. When  $d = 0$ , which means CSRR is a closed ring, the original resonance disappears. At this time, the antenna only works in S-band. As displayed in **Figure 2C**, when  $\theta$  increases from 0 to 45°, the original resonance frequency moves to the lower frequency. Moreover, when  $\theta = 30^\circ$ , the return loss at the original resonance frequency reaches maximum. **Figure 2D** depicts that, as  $h$  increases from 24.0 to 25.5 mm, the new resonance frequency moves to the lower frequency. When  $h = 24.5$  mm, the return loss at new resonance point is at its maximum, now the centers of CSRR and the substrate coincide. Considering the performance of antenna comprehensively, we designed the ground plane of the proposed antenna as **Figure 1D**. The parameters of the proposed antenna are listed in **Table 1**.





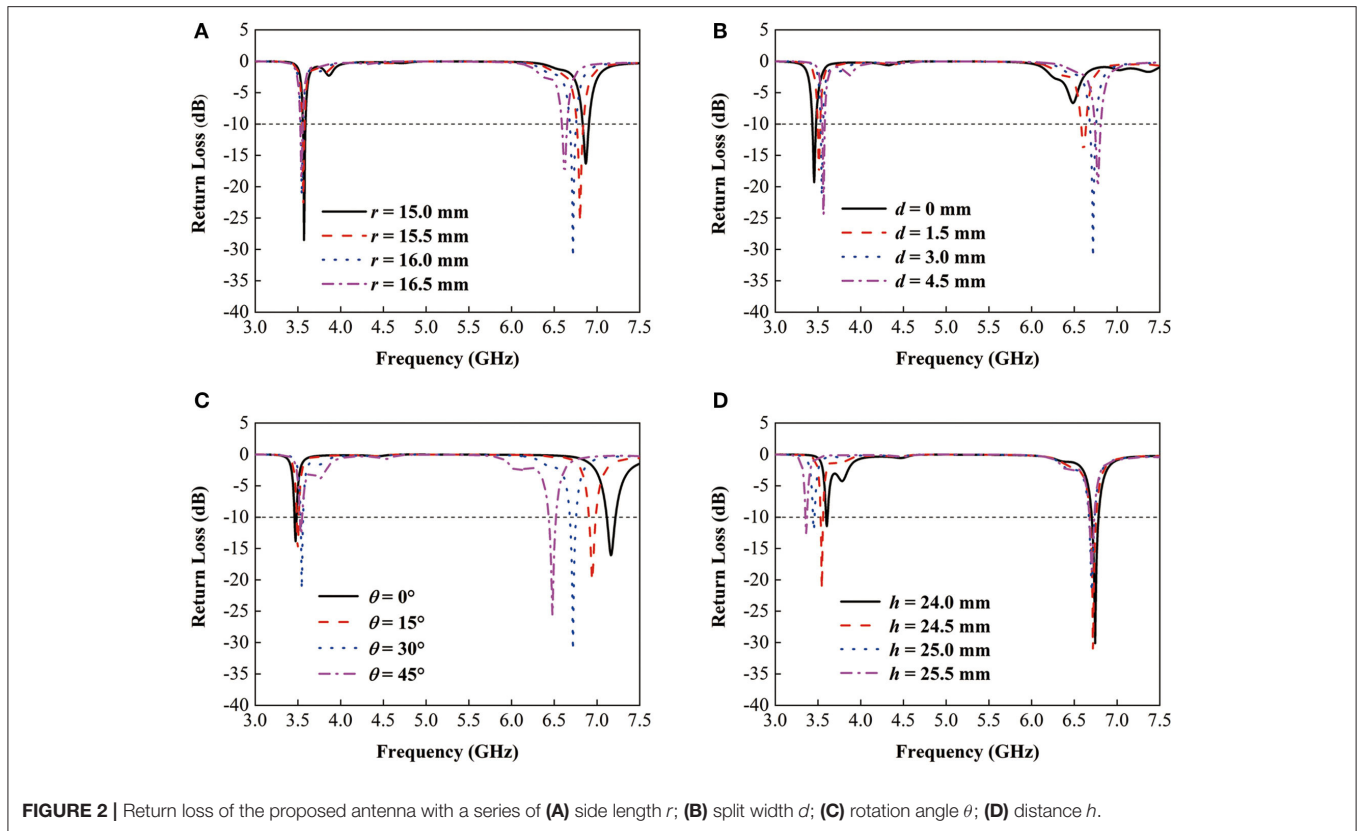


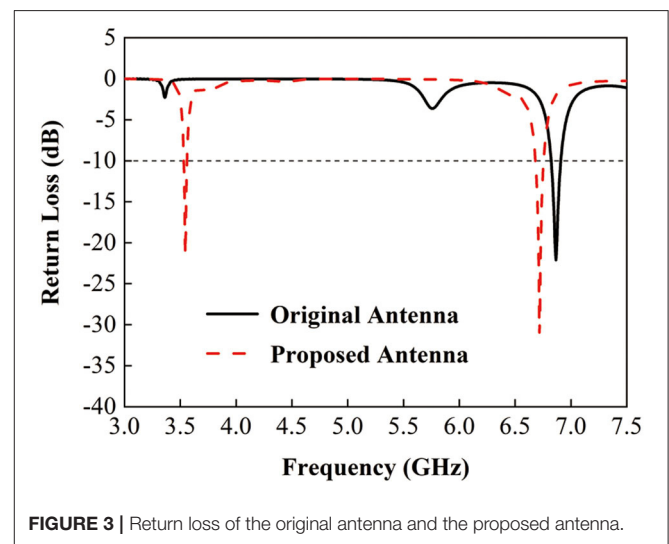
**TABLE 1 |** Parameters of the proposed antenna.

Parameter	Value	Parameter	Value
$a$	40.0 mm	$b$	49.0 mm
$t$	1.5 mm	$w$	22.5 mm
$wf_1$	1.5 mm	$wf_2$	1.0 mm
$t_1$	0.035 mm	$l_1$	14.0 mm
$l_2$	14.0 mm	$l_3$	14.0 mm
$r$	16.0 mm	$d$	3.0 mm
$s$	1.0 mm	$h$	24.5 mm
$\theta$	30°		

To intuitively illustrate the effect of CSRR on the antenna frequency band, the return loss of the original antenna and the proposed antenna are compared. As shown in **Figure 3**, it can be inferred that the proposed antenna has a new resonance peak centered at 3.54 GHz with a return loss of 21.4 dB. The original resonance frequency shifts from 6.87 to 6.72 GHz, and its return loss increases from 22.1 to 31.2 dB.

## RESULTS AND DISCUSSION

In order to explain the work principle of CSRR, the surface current distribution of the antenna is observed. **Figure 4** shows the surface current distribution of the antenna without CSRR at 6.87 and 5.00 GHz. From **Figures 4A,B**, we can see that the current density at 6.87 GHz is higher than 5.00 GHz. It can be



deduced that the electromagnetic wave of a specific frequency is excited by the rectangular patch and the feedlines, resulting in resonance at 6.87 GHz.

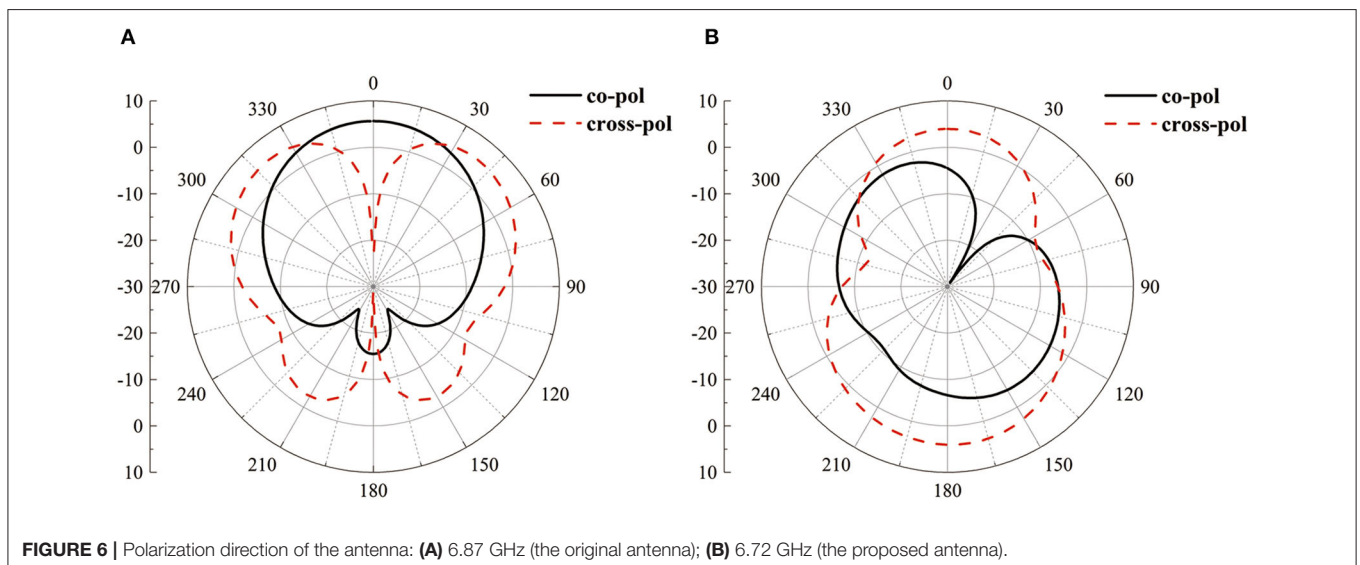
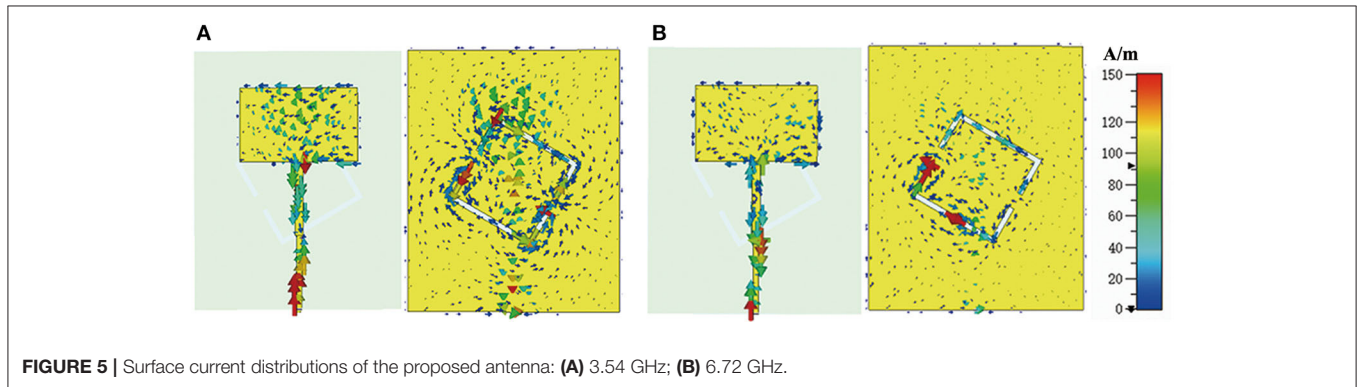
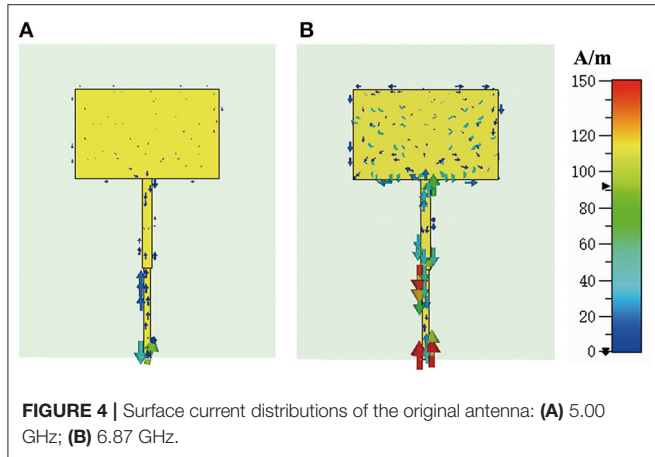
**Figure 5** shows the surface current distribution of the antenna with CSRR at two resonance frequencies. It can be observed that the current is no longer limited between the radiation patch and feedlines. It also distributes around CSRR, which demonstrates that the CSRR can act as a resonator to generate new resonance peak. Obviously, etching CSRR damages the structure of the

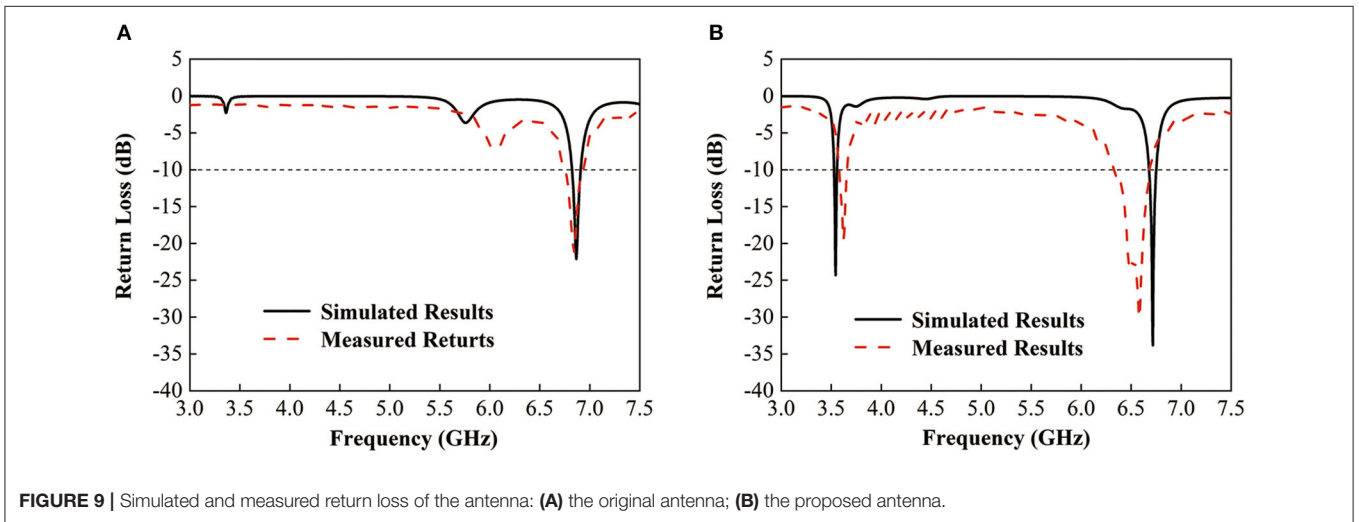
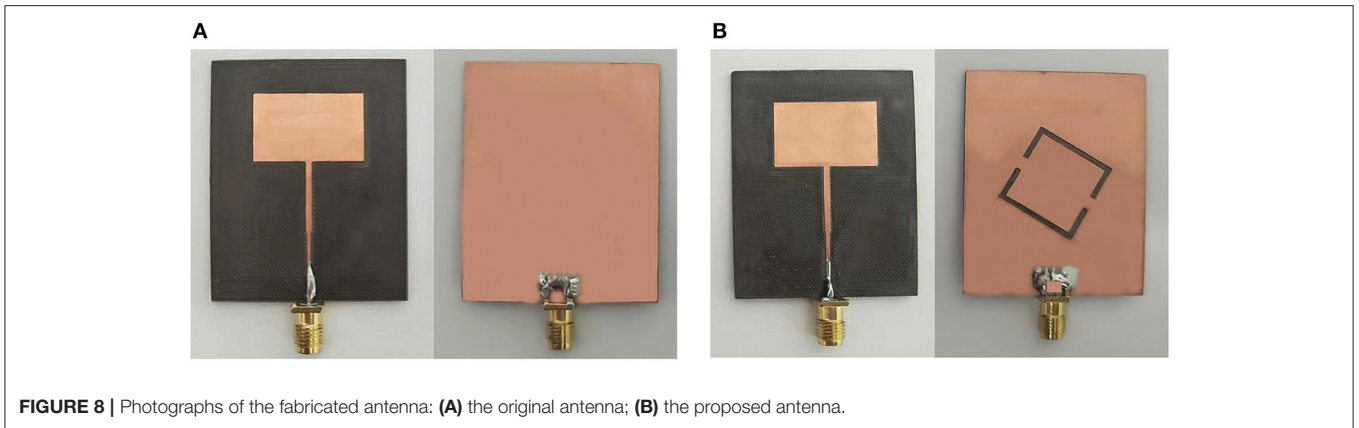
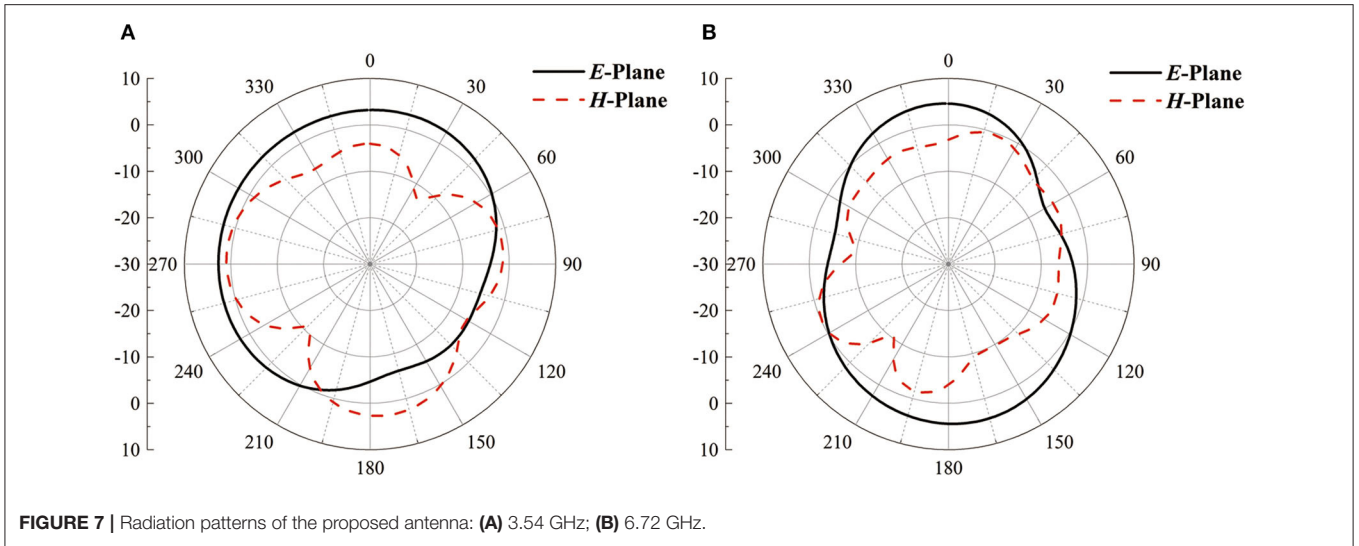
ground plane, so that the current distribution is changed. Moreover, the current shocks back and forth in the CSRR, radiating a specific frequency of electromagnetic wave. However, there are some differences in the surface current distribution of **Figures 5A,B**. At the frequency of 3.54 GHz, the surface current

mainly distributes around the CSRR. Thus, the new generated resonance peak is mainly affected by the parameters of the CSRR. Similarly, the resonance peak centered at 6.72 GHz is modulated by the rectangle patch and CSRR.

In order to figure out why CSRR can be used as a resonator, a few more details are exhibited. Comparing the results shown in **Figure 5**, it can be observed that the surface current distributes around the whole CSRR at 3.54 GHz, while only the lower half of CSRR has a current distribution at 6.72 GHz. It can be inferred that CSRR serves as a frequency-controlled switch which only opens at specific frequencies. When the switch is closed, the current in the CSRR shocks back and forth, resulting in new resonance within the antenna at 3.54 GHz. When the switch is on, the electromagnetic wave is only generated by the lower section of CSRR and it couples with the antenna radiating element, resulting in the original resonance point shifting by  $\sim 0.15$  GHz. Combining with the return loss diagram in **Figure 3**, it can be concluded that the return loss at the resonance frequency increases by  $\sim 40\%$ .

CSRR can not only produce resonance peaks as a resonator, but also affect the radiation characteristics of the antenna. To analyze the effect of CSRR on the polarization mode, the





polarization direction of the antenna with and without CSRR are shown in **Figure 6**. **Figure 6A** shows that the polarization direction of the antenna without CSRR is symmetrical at 6.87

GHz, while **Figure 6B** indicates that the symmetry of the antenna with CSRR is broken at 6.72 GHz. It can be interpreted that the polarization mode of antenna is highly related to its

**TABLE 2** | Comparison of the antenna performances of this work and the previous literatures.

References	Antenna size (mm <sup>2</sup> )	Number of resonance peaks	Operating frequency band	Resonance frequencies (GHz)/ Peak gain (dBi)
[8]	50 × 58	4	S, C, X	2.1/1.30 3.3/1.59 5.3/2.12 7.5/3.73
[14]	5 × 5	1	C	—
[22]	60 × 60	3	S, C	2.45/1.03 3.56/5.10 5.60/5.41
This work	40 × 49	2	S, C	3.54/4.78 6.72/4.65

structure and changes within the structure. In order to better evaluate the antenna performance, the radiation patterns of the proposed antenna at resonance points are investigated as shown in **Figure 7**. It can be seen that the radiation patterns in *H*-Plane are almost omnidirectional and the radiation patterns in *E*-Plane are monopole-like. In addition, the distortion of the radiation patterns is extremely slight, which proves that the introduction of CSRR has almost no effect on the performance of the antenna.

To verify the simulated results, the original antenna and the proposed antenna are fabricated, measured, and compared. A circuit board engraving machine is used to fabricate the antenna and a vector network analyzer (VNA) is used to measure the electromagnetic properties of the antenna. The fabricated antenna are shown in **Figure 8**. The simulated and measured return loss of the original antenna and the proposed antenna are shown in **Figure 9**. From **Figure 9A**, the two curves have a nearly consistent trend and the resonance peaks almost coincide. As depicted in **Figure 9B**, the two measured resonance frequencies move from 3.54 and 6.72 GHz to 3.62 and 6.58 GHz, respectively. Compared with the simulated curves, the return loss decreases by 3–4 dB. Considering the inevitable errors in the process of antenna manufacturing, welding, and measuring, the above deviation can be ignored. Similarly, the fact that the bandwidth of measured curves is broader than the simulated curves is also due to fabrication and measurement errors. Therefore, the measured results correlate with the simulated ones, which proves the reliability of the antenna.

## REFERENCES

1. El-Halaoui M, Kaabal A, Asselman H, Ahyoud S, Asselman A. Multiband planar inverted-F antenna with independent operating bands control for mobile handset applications. *Int J Antennas Propag.* (2017) **2017**:8794039. doi: 10.1155/2017/8794039
2. Huang S, Guo B, Liu Y. 5G-oriented optical underlay network slicing technology and challenges. *IEEE Commun Mag.* (2020) **58**:13. doi: 10.1109/MCOM.001.1900583

Based on the above analysis, it can be summarized that an antenna etched with CSRR performs excellently despite being small in size and containing a simple structure. Furthermore, we compared the dual-band antenna designed in this work with other literature [8, 14, 22] in terms of size, number of resonance peaks, operating frequency bands, and peak gain, as listed in **Table 2**. It is observed that, in other works, multi-band antenna are larger, while small size antenna operate at single-band. The design of our work realizes both miniaturization and multi-band in an antenna, which widens the possibilities for multi-band antenna design.

## CONCLUSION

In conclusion, a dual-band MPA etched with CSRR was designed. The proposed antenna with high performance was obtained by optimizing the structural parameters of CSRR. Based on the simulated results of surface current distribution, it was found that the current shocks back and forth in the CSRR, generating a new resonance peak. By adjusting the rotation angle of the CSRR, an obvious resonance frequency appears. Moreover, the consistency between the simulation and the recorded measurement demonstrates the validity of the design. This work provides a new way to design multi-band antenna.

## DATA AVAILABILITY STATEMENT

The raw data supporting the conclusions of this article will be made available by the authors, without undue reservation.

## AUTHOR CONTRIBUTIONS

HY, KB, and XL designed the structure and fabricated the sample. HZ and HL performed the experiments. HY, HL, and KB wrote the manuscript with contribution from all the other authors. All authors participated in the discussion of the results.

## FUNDING

This work was supported by the National Natural Science Foundation of China (Grant Nos. 51972033, 61774020, 51788104, 61672108, 11574311, and 61976025), Science and Technology Program of Shenzhen Science and Technology Innovation Commission (Grant Nos. JCYJ20180306173235924 and JCYJ20180305164708625).

3. Montalvao ESR, Montalvao ACPS, Campos ALPS, Gomes Neto A. A new model of metasurface used for linear-to-circular polarization conversion in antenna array. *Microw Opt Technol Lett.* (2016) **58**:861. doi: 10.1002/mop.29681
4. Yu Z, Yu JG, Ran XY, Zhu CH. A novel ancient coin-like fractal multiband antenna for wireless applications. *Int J Antennas Propag.* (2017) **2017**:6459286. doi: 10.1155/2017/6459286
5. Xu J, Guo Y, Yang P, Zhang R, Zhai X, Huang S, et al. Recent progress on RF orbital angular momentum antennas. *J Electromagnet Wave.* (2020) **34**:275. doi: 10.1080/09205071.2019.1708814



6. Zhang ZJ, Zhang WY, Zeadally S, Wang YA, Liu Y. Cognitive radio spectrum sensing framework based on multi-agent architecture for 5G networks. *IEEE Wirel Commun.* (2015) **22**:34–9. doi: 10.1109/MWC.2015.7368822
7. Ran XY, Yu Z, Xie TY, Li Y, Wang XX, Huang P. A novel dual-band binary branch fractal bionic antenna for mobile terminals. *Int J Antennas Propag.* (2020) **2020**:6109093. doi: 10.1155/2020/6109093
8. Kumar A, Sankhla V, Deegwal JK, Kumar A. An offset CPW-fed triple-band circularly polarized printed antenna for multiband wireless applications. *AEU-Int J Electron Commun.* (2018) **86**:133–41. doi: 10.1016/j.aeue.2018.02.002
9. Akhtar F, Naqvi SI, Arshad F, Amin Y, Tenhunen H. A flexible and compact semicircular antenna for multiple wireless communication applications. *Radioengineering.* (2018) **27**:671–8. doi: 10.13164/re.2018.0671
10. Chen Y, Ye LF, Zhuo JL, Liu YH, Zhang L, Zhang M, et al. Frequency reconfigurable circular patch antenna with an arc-shaped slot ground controlled by PIN diodes. *Int J Antennas Propag.* (2017) **2017**:7081978. doi: 10.1155/2017/7081978
11. Ullah S, Ahmad S, Khan BA, Tahir FA, Flint JA. An hp-shape hexa-band antenna for multi-standard wireless communication systems. *Wirel Netw.* (2019) **25**:1361–9. doi: 10.1007/s11276-018-1760-x
12. Zhao Y. Design of high-gain, wideband antenna using microwave hyperbolic metasurface. *AIP Adv.* (2016) **6**:055022. doi: 10.1063/1.4952752
13. Xu J, Bi K, Zhang R, Hao Y, Lan C, McDonald-Maier K, et al. A small-divergence-angle orbital angular momentum metasurface antenna. *Research.* (2019) **2019**:9686213. doi: 10.34133/2019/9686213
14. Almutairia AF, Islam MS, Samsuzzaman M, Islam MT, Misran N, Islam MT. A complementary split ring resonator based metamaterial with effective medium ratio for C-band microwave applications. *Results Phys.* (2019) **15**:102675. doi: 10.1016/j.rinp.2019.102675
15. Xu JC, Hao YN, Bi K, Zhang R, Huang SG, Zhou J. Microwave orbital angular momentum beam generation based on circularly polarized metasurface antenna array. *Eng Sci.* (2019) **6**:30–35. doi: 10.30919/es8d748
16. Patel SK, Kosta YP. Meandered multiband metamaterial square microstrip patch antenna design. *Wave Random Complex.* (2012) **22**:475–87. doi: 10.1080/17455030.2012.723837
17. Fu X, Cui T. Recent progress on metamaterials: From effective medium model to real-time information processing system. *Prog Quant Electron.* (2019) **67**:100223. doi: 10.1016/j.pquantelec.2019.05.001
18. Xu JC, Tao L, Zhang R, Hao YN, Huang SG, Bi K. Broadband complementary ring-resonator based terahertz antenna. *Opt Express.* (2017) **25**:17099–104. doi: 10.1364/OE.25.017099
19. Patel SK, Argyropoulos C, Kosta YP. Broadband compact microstrip patch antenna design loaded by multiple split-ring resonator superstrate and substrate. *Wave Random Complex.* (2017) **27**:92–102. doi: 10.1080/17455030.2016.1203081
20. Gupta A, Bansal B, Mishra VK, Agrawal A. Miniaturised tri-band rhombus-shaped metamaterial-inspired antenna with gain enhancement using complementary closed ring resonators. *IET Microw Antennas Propag.* (2020) **14**:185–93. doi: 10.1049/iet-map.2019.0567
21. Patchala K, Raja-Rao Y, Prasad AM. Triple band notch compact MIMO antenna with defected ground structure and split ring resonator for wideband applications. *Heliyon.* (2020) **6**:e03078. doi: 10.1016/j.heliyon.2019.e03078
22. Ali W, Hamad E, Bassiuny M, Hamdallah M. Complementary split ring resonator based triple band microstrip antenna for WLAN/WiMAX applications. *Radioengineering.* (2017) **26**:78–84. doi: 10.13164/re.2017.0078
23. Zhou C, Wang GM, Wang YW, Zong BF, Ma J. CPW-Fed dual-band linearly and circularly polarized antenna employing novel composite right/left-handed transmission-line. *IEEE Antennas Wirel Propag Lett.* (2013) **12**:1073–6. doi: 10.1109/LAWP.2013.2279689
24. Xu J, Li RQ, Jiang XP, Wang SY, Han TC. Ultra-wideband linear polarization converter based on square split ring. *Acta Phys Sin.* (2019) **68**:117801. doi: 10.7498/aps.68.20190267
25. Tao L, Xu JC, Li HH, Hao YN, Huang SG, Lei M, et al. Bandwidth enhancement of microstrip patch antenna using complementary rhombus resonator. *Wirel Commun Mob Com.* (2018) **2018**:6352181. doi: 10.1155/2018/6352181
26. Lan JX, Cao XY, Gao J, Han JF, Liu T, Cong LL, et al. Novel design of microstrip antenna array with low scattering performance. *Acta Phys Sin.* (2019) **68**:034101. doi: 10.7498/aps.68.20181708

**Conflict of Interest:** The authors declare that the research was conducted in the absence of any commercial or financial relationships that could be construed as a potential conflict of interest.

Copyright © 2020 Yao, Liu, Zhu, Li, Dong and Bi. This is an open-access article distributed under the terms of the Creative Commons Attribution License (CC BY). The use, distribution or reproduction in other forums is permitted, provided the original author(s) and the copyright owner(s) are credited and that the original publication in this journal is cited, in accordance with accepted academic practice. No use, distribution or reproduction is permitted which does not comply with these terms.